

Frequency-selective beamforming and single-shot beam training with dynamic metasurface antennas

Nitish Vikas Deshpande, *Student Member, IEEE*, Joseph Carlson, Miguel R. Castellanos, *Member, IEEE*, and Robert W. Heath Jr., *Fellow, IEEE*

Abstract—Dynamic metasurface antennas (DMAs) beamform through low-powered components that enable reconfiguration of each radiating element. Previous research on a single-user multiple-input-single-output (MISO) system with a dynamic metasurface antenna at the transmitter has focused on maximizing the beamforming gain at a fixed operating frequency. The DMA, however, has a frequency-selective response that leads to magnitude degradation for frequencies away from the resonant frequency of each element. This causes reduction in beamforming gain if the DMA only operates at a fixed frequency. We exploit the frequency reconfigurability of the DMA to dynamically optimize both the operating frequency and the element configuration, maximizing the beamforming gain. We leverage this approach to develop a single-shot beam training procedure using a DMA sub-array architecture that estimates the receiver’s angular direction with a single OFDM pilot signal. We evaluate the beamforming gain performance of the DMA array using the receiver’s angular direction estimate obtained from beam training. Our results show that it is sufficient to use a limited number of resonant frequency states to do both beam training and beamforming instead of using an infinite resolution DMA beamformer.

Index Terms—Dynamic metasurface antenna, resonant frequency, frequency-selective beamforming, beam training

I. INTRODUCTION

While most prior work on DMAs assumes frequency-flat operation, their inherent ability to reconfigure beamforming properties over a wide bandwidth makes them promising candidates for frequency-selective wireless architectures [1], [2]. A DMA consists of a waveguide with multiple radiating slots that can be independently tuned to resonate at different frequencies [3], [4]. Unlike conventional antenna arrays that require external components for beamforming, DMAs have the innate capability to beamform through low-powered varactor or PIN diodes embedded into the antennas [4]. Conventional analog components for frequency-selective beamforming such as true time delay (TTD) elements [5] and phase-shifters [6] consume more power than varactor or PIN diodes [7]. The low cost and low power consumption of DMAs make them highly versatile, with potential applications such as large

array implementations in gNBs or use in battery-limited UE handsets.

DMAs present a unique set of challenges for beamforming compared to a traditional phased-array architecture because of the differences in their underlying operation mechanism. The magnitude and phase response of each radiating slot in the DMA is coupled. The DMA architecture also has an intrinsic phase-advance in the waveguide. Furthermore, the underlying mechanism for beamforming in fact makes the beamforming frequency-selective. The operating bandwidth and extent of frequency selectivity are tightly coupled together in the design [2]. As a result, even a task like configuring a DMA to produce a directive beam for a line-of-sight channel is deceptively complicated.

Prior work on DMA signal processing is limited to optimizing narrowband metrics. The design of beamforming algorithms with DMAs is non-trivial because of the coupled magnitude and phase constraint, also referred to as the Lorentzian constraint in [4]. One approach to configure DMA beamforming weights is to relax the Lorentzian constraint, solve for the desired phase-shift, and project the obtained weight on the set of feasible weights on the Lorentzian circle [8]. This relaxation and projection approach was shown to be sub-optimal in [9] which proposed another solution based on an optimal common phase rotation to each slot on the DMA. The single-user solution was generalized to a multi-user downlink system in [10], uplink system in [11] and [12], and hybrid beamforming with the DMA in [13] and [14]. The DMA beamforming approaches in [8]–[14] treat the DMA beamforming weights as frequency-flat, i.e., the phase and magnitude response as a function of frequency is not explicitly modeled. Hence, this prior work on DMA is not directly applicable for wideband scenarios where DMA frequency-selectivity and beam squint is significant. Although frequency-reconfigurable antennas have been proposed for wireless systems with multi-band capabilities [15], [16], there is limited prior work on analyzing frequency-selective beamforming with DMAs. In [17], a DMA-based MIMO-OFDM system was analyzed by modeling the frequency-selectivity profile of the DMAs. Their approach, however, does not compare frequency-selective DMA beamforming with traditional TTD or phased-array architectures. In this paper, we bridge this gap by proposing a method to configure DMAs to achieve maximum beamforming gain comparable to TTD or phased-array systems.

In our paper, we leverage the ability of the DMA to be dynamically reconfigured over a wide frequency range to

Nitish Vikas Deshpande, Joseph Carlson, and Robert W. Heath Jr. are with the Department of Electrical and Computer Engineering, University of California San Diego, La Jolla, CA 92093 USA (e-mail: nideshpande@ucsd.edu; j4carlson@ucsd.edu; rwheathjr@ucsd.edu). Miguel R. Castellanos is with the Department of Electrical Engineering and Computer Science at the University of Tennessee, Knoxville, TN 37996 USA (e-mail: mrcastellanos@utk.edu). This material is based upon work supported by the National Science Foundation under grant nos. NSF-ECCS-2435261, NSF ECCS-2414678, the Army Research Office under Grant W911NF2410107, and the Qualcomm Innovation Fellowship.

make the DMA performance comparable to the conventional architectures. We envision a wireless system with DMA that has the ability to be reconfigured to different subcarrier frequencies. In current wireless standards, there exist methods that can dynamically adapt the operating frequency for several applications. For example, in 5G NR, techniques like dynamic spectrum sharing allows the base station to dynamically switch between different frequency bands depending on the network load and user demand [18]. Adaptive frequency hopping is used in Bluetooth to avoid interference, with the system able to operate at different frequency bands [19]. Taking motivation from the current standards, our proposed method for DMA beamforming allows the system operator to dynamically choose the DMA operating frequency within a feasible band. This enables configuring the DMA resonant frequencies based on the selected operating frequency. We propose a two-stage optimization framework where the operating frequency is also an optimization variable. The first stage of the algorithm configures the DMA resonant frequencies to maximize the beamforming gain at a specific operating frequency, expressing the optimal resonant frequencies as a closed-form parametric function of the operating frequency. The second stage of the algorithm optimizes over all operating frequencies in the feasible operating band. This approach is suitable for systems with spectrum availability similar to the DMA operating range, allowing for the selection of operating frequencies for communication. Our novel contribution is the second stage of optimizing the operating frequency, which mitigates the impact of magnitude degradation on the DMA beamforming weight. With this frequency-selective strategy, the beamforming gain and hence achievable rate improves compared to prior work [4], [9], [10], [12]. We further show that by optimal design choice for the DMA waveguide refractive index and inter-element spacing, the maximum beamforming gain for the DMA architecture equals that of a TTD array within the desired angular range.

To achieve the desired beamforming gain at the receiver, the transmit DMA array requires a good estimate of the receiver's angular direction. The second contribution of our paper is a beam training procedure for DMAs to estimate the receiver's angular direction. We demonstrate that with a DMA array, single-shot beam training is possible by leveraging the frequency reconfiguration property. Although single-shot beam training has been studied for TTD arrays [20], [21] and a leaky waveguide antenna [22], it has not been analyzed for DMAs in prior work. We propose a beam training procedure that probes different directions simultaneously using different subcarrier frequencies in a sub-array approach for the DMA array.

We summarize the key novelties of our paper with respect to prior work. We formulate the frequency-selective DMA beamforming gain optimization for a line-of-sight channel. To make the maximum achievable DMA gain the same as that of TTD, we propose selecting the optimal operating frequency based on the receiver's angular direction unlike prior work which is limited to a single frequency optimization. We propose a single-shot beam training procedure for a DMA planar array using a sub-array approach that enables the system to probe multiple angles simultaneously with a single OFDM

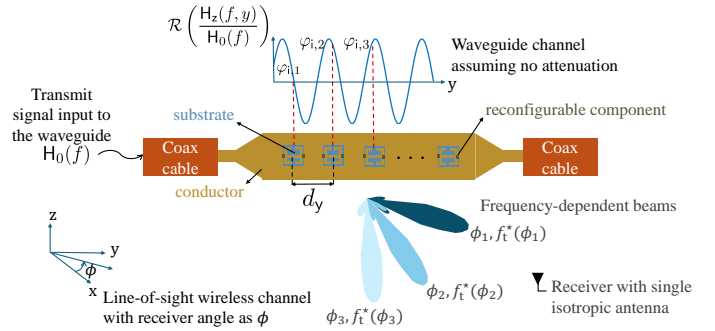


Fig. 1: A DMA has radiating slots which are tuned using low-power reconfigurable components with signal incident from one end of the waveguide. We leverage the frequency reconfigurability property of DMA for frequency-selective beamforming.

symbol. We compare the beamforming gain for two cases: (i) perfectly known receiver's angular direction, and (ii) angular direction estimated via the proposed training. We demonstrate that the second case, using a finite set of resonant frequencies, performs comparably to the first, which requires infinite frequency resolution. We show that the optimal operating frequency approach outperforms the benchmarks based on the fixed center frequency approach for all DMA operating frequency ranges. We also obtain an achievable rate of DMA that is comparable to a TTD array up to a certain bandwidth.

Our paper is organized as follows. We study a communication system where the transmitter is equipped with a DMA and the receiver has a single isotropic antenna. We discuss the single DMA transmitter model in Section II-A, formulate the propagation channel model and the received signal model in Section II-B, and define the signal-to-noise ratio (SNR) and achievable rate in Section II-C. In Section III, we analyze the beamforming gain for the single DMA transmitter. In Section IV, we generalize the results of Section III to multiple DMAs arranged as a planar array, propose the single-shot beam training procedure, and a beam training codebook design. In Section V, we evaluate the achievable rate DMA performance and compare with existing approaches. The MATLAB simulation code to generate the results is made publicly available to facilitate reproducibility¹.

Universal constants: Speed of light $c = 3 \times 10^8$ [m/sec], intrinsic impedance of free space $\eta_0 \approx 377 \Omega$, Boltzmann constant $k_B = 1.38 \times 10^{-23}$ J/K.

Notation: A bold lowercase letter \mathbf{h} denotes a column vector, $(\cdot)^T$ denotes transpose, $|\cdot|$ indicates absolute value, \odot represents the element-wise product, $\text{sgn}(\cdot)$ indicates the *signum* function, $\mathbf{1}$ be the all-ones vector.

II. SYSTEM MODEL

A. Model of a single DMA transmitter

We describe the model of a single DMA at the transmitter. A DMA is a type of a metasurface antenna that has reconfigurable radiating slots on the upper surface of a conducting

¹<https://github.com/nvdeshpa/FreqSelBeamformingBeamtrainingDMAs>

waveguide. Let the DMA be in the yz plane as illustrated in Fig. 1. The transmit signal enters the DMA from the waveguide input and propagates along its length. We assume the DMA has N equally spaced radiating slots with inter-element spacing d_y along the y axis. DMAs function as leaky-wave antennas with reconfigurable components like varactor or PIN diodes attached to the radiating slots to tune slot resonant frequencies. As the signal travels along the waveguide, each slot experiences a different magnitude and phase of the input signal. The input signal radiates out of each slot, and the phase and magnitude of the transmit signal can be tuned by adjusting the slot resonant frequency. Through this mechanism, DMAs have the capability to adjust the transmit signal without external phase-shifters or delay elements.

The data signal is contained in the EM field entering the waveguide. Let $H_0(t)$ [A/m] be the time domain representation of the transverse magnetic field strength at the waveguide input. For a mathematically tractable analysis of achievable rate, we assume that the data signal is a Gaussian wide-sense stationary random process that is completely described by its mean and second-order moment [23]. This signal does not have a finite energy and a windowed Fourier Transform with interval T_0 is used to define its spectrum [24]. We use the passband frequency f in Hertz for frequency-domain representation. Let the frequency domain magnetic field be $H_0(f) = \int_{-\frac{T_0}{2}}^{\frac{T_0}{2}} H_0(t)e^{-j2\pi ft} dt \left[\frac{\text{A/m}}{\text{Hz}} \right]$. This frequency domain representation allows analysis of the EM fields in a communication-theoretic framework.

We use the polarizable dipole framework in [4] to model the radiation characteristics of the DMAs. The DMA radiating slots are much smaller compared to the free-space wavelength and can be modeled as reconfigurable magnetic dipoles along the y axis. Each magnetic dipole has a frequency-selective response governed by its magnetic polarizability, which connects the induced magnetic dipole moment with the magnetic field propagating inside the waveguide. Let $\alpha_{M,n}(f)$ [m^3] be the frequency response of the magnetic polarizability of the dipole corresponding to the n th element on the DMA [25]. Unlike a conventional dipole array where each element is excited independently, each dipole is excited by the transverse magnetic field as it propagates along the DMA.

We characterize the magnetic polarizability using the Lorentzian model from [4]. This model captures the resonant behavior of the elements on the DMA. Let F [m^3] be the coupling factor and Γ [Hz] be the damping factor in the Lorentzian model. Let $f_{r,n}$ be the resonant frequency for the n th dipole that is dynamically reconfigurable. The Lorentzian expression for the magnetic polarizability is [4]

$$\alpha_{M,n}(f) = \frac{F2\pi f^2}{2\pi f_{r,n}^2 - 2\pi f^2 + j\Gamma f} [\text{m}^3]. \quad (1)$$

We assume that F and Γ are fixed and dependent on the DMA unit cell design.

The polarizability can also be defined in terms of the quality factor $Q = \frac{2\pi f}{\Gamma}$. Let the complex argument of the polarizability be denoted as $\psi_n(f)$ and be defined as

$$\psi_n(f) = \text{atan2}(-\Gamma f, 2\pi(f_{r,n}^2 - f^2)). \quad (2)$$

Using the definition of quality factor and (2), we express the magnetic polarizability from (1) as

$$\alpha_{M,n}(f) = -FQ \sin(\psi_n(f)) e^{j\psi_n(f)} [\text{m}^3]. \quad (3)$$

We see that the reconfigurable resonant frequency $f_{r,n}$ modifies both the phase and magnitude of the magnetic polarizability. The key insight from (3) is that the phase and magnitude of the magnetic polarizability are coupled and cannot be tuned independently.

We model the change in the excitation signal in the DMA waveguide as it propagates by a relative phase difference between the excitation of each polarizable dipole. For a simplified analysis, we assume that there is no attenuation of the field inside the waveguide so that the excitation amplitude is uniform across all DMA elements [4]. Including the attenuation in the model leads to a loss in the DMA beamforming gain which we discuss later in the numerical results in Section III-D. The relative phase of the excitation at the n th dipole is $e^{j\varphi_{i,n}(f)}$, which we term as the intrinsic phase-shift. It is dependent on the waveguide refractive index and inter-element spacing of the DMA radiating slots, and cannot be dynamically adjusted. Similar to [4], we assume that the transverse magnetic field component is sinusoidal in terms of the distance traveled along the y axis. We denote the refractive index by n_g , where subscript g is used to indicate the waveguide. The z component of the waveguide magnetic field with constant magnitude $|H_0(f)|$ is expressed as $H_z(f, y) = H_0(f)e^{-jn_g 2\pi \frac{f}{c} y} \left[\frac{\text{A/m}}{\text{Hz}} \right]$. The data signal incident on each radiating slot is governed by $H_z(f, y)$.

The radiating slots along the y axis sample $H_z(f, y)$ at an interval of d_y as shown in Fig. 1. The induced magnetic dipole moment $m_z(f, y_n)$ [$\frac{\text{Am}^2}{\text{Hz}}$] along the z axis for the n th radiating slot located at distance y_n from the waveguide input is

$$m_z(f, y_n) = H_z(f, y_n)\alpha_{M,n}(f) = H_0(f)e^{-jn_g 2\pi \frac{f}{c} y_n} \alpha_{M,n}(f). \quad (4)$$

Without loss of generality, let the intrinsic phase-shift at the first element placed at the origin be 0. We express the intrinsic phase-shift at the n th element as

$$\varphi_{i,n}(f) = -n_g 2\pi \frac{f}{c} (n-1)d_y, \quad (5)$$

and define the waveguide phase-shift vector as $\mathbf{h}_{\text{dma}}(f) = [e^{j\varphi_{i,1}(f)}, \dots, e^{j\varphi_{i,N}(f)}]^T$. The waveguide phase-shift vector accounts for the phase-difference between the excitation at different slots.

B. Received signal model

Now, we describe the wireless propagation channel between the DMA transmitter and the single antenna receiver. The phase-shift due to wireless propagation at the n th slot on the transmit DMA is denoted as $e^{j\varphi_{e,n}(\phi, f)}$. Assuming a line-of-sight and far-field propagation where the receiver is at an azimuth angle ϕ from the broadside direction (x axis in Fig. 1), the extrinsic phase-shift angle at the n th element is $\varphi_{e,n}(\phi, f) = -2\pi \frac{f}{c} (n-1)d_y \sin(\phi)$. Let the far-field array response vector be $\mathbf{a}(\phi, f) = [e^{j\varphi_{e,1}(\phi, f)}, \dots, e^{j\varphi_{e,N}(\phi, f)}]^T$.

Note that the extrinsic phase-shift angle $\varphi_{e,n}(\phi, f)$ depends on the transmit angle of departure (AoD) ϕ which can vary unlike the intrinsic phase-shift angle $\varphi_{i,n}(f)$ that depends only on the fixed DMA waveguide design.

The effective propagation channel is expressed as $\mathbf{h}(\phi, f) = \mathbf{h}_{\text{dma}}(f) \odot \mathbf{a}(\phi, f)$. The phase of the n th element in $\mathbf{h}(\phi, f)$ is

$$\varphi_n(\phi, f) = \varphi_{i,n}(f) + \varphi_{e,n}(\phi, f) \quad (6)$$

$$= -2\pi \frac{f}{c} (n-1) d_y (n_g + \sin(\phi)). \quad (7)$$

For a conventional array, $\varphi_{i,n}(f) = 0$. Hence, $\varphi_n(\phi, f) = \varphi_{e,n}(\phi, f)$. For a matched filter strategy, this implies applying an equal and opposite phase-shift $\varphi_{r,n}(\phi, f) = -\varphi_{e,n}(\phi, f)$ to beamform toward ϕ . For a DMA, the transmit beamforming should account for the additional term $\varphi_{i,n}(f)$ in the overall phase.

We define the received power spectral density in terms of the transmit power spectral density. Assuming that mutual coupling is negligible between each radiating slot, the far-field component of the electric field at the receiver in the xy plane at a distance r from the DMA is [4]

$$\begin{aligned} E_\phi(f) &= \eta_0 \left(\frac{2\pi f}{c} \right)^2 \sum_{n=1}^N m_z(f, y_n) \frac{e^{j\varphi_{e,n}(\phi, f)}}{4\pi r} \left[\frac{\text{V/m}}{\text{Hz}} \right], \\ &\stackrel{(a)}{=} \frac{\eta_0}{4\pi r} \left(\frac{2\pi f}{c} \right)^2 H_0(f) \sum_{n=1}^N \alpha_{M,n}(f) e^{j\varphi_n(\phi, f)} \left[\frac{\text{V/m}}{\text{Hz}} \right]. \end{aligned} \quad (8)$$

Here, equality (a) follows from (4) and (6) by substituting the expression of the induced magnetic dipole moment.

The receive electric field shows how the polarizability terms beamform the signal from each slot. To make the analysis consistent with traditional beamforming, we define the dimensionless DMA beamforming vector as

$$\mathbf{f}_{\text{DMA}}(f) = \left[-\sin(\psi_1(f)) e^{j\psi_1(f)}, \dots, -\sin(\psi_N(f)) e^{j\psi_N(f)} \right]^T \quad (9)$$

This yields

$$E_\phi(f) = \frac{\eta_0}{4\pi r} \left(\frac{2\pi f}{c} \right)^2 H_0(f) \text{FQ} \mathbf{f}_{\text{DMA}}^T(f) \mathbf{h}(\phi, f) \left[\frac{\text{V/m}}{\text{Hz}} \right]. \quad (10)$$

Similarly, the far-field magnetic field strength component perpendicular to the xy plane is $H_\theta(f) = -\frac{1}{\eta_0} E_\phi(f) \left[\frac{\text{A/m}}{\text{Hz}} \right]$. The radial component of the Poynting vector is

$$\begin{aligned} S_r(f) &= -\frac{1}{2} E_\phi(f) H_\theta^c(f) = \frac{\eta_0}{2} |H_\theta(f)|^2 \left[\frac{\text{W/m}^2}{\text{Hz}^2} \right], \quad (11) \\ &= \frac{1}{4\pi r^2} \frac{\eta_0}{8\pi} \left(\frac{4\pi^2 f^2 |H_0(f)| \text{FQ} |\mathbf{f}_{\text{DMA}}^T(f) \mathbf{h}(\phi, f)|}{c^2} \right)^2 \left[\frac{\text{W}}{\text{m}^2 \text{Hz}^2} \right]. \end{aligned} \quad (12)$$

Let the transmit power spectral density be defined as $P_T(f) = \lim_{T_0 \rightarrow \infty} \frac{1}{T_0} \frac{\eta_0}{8\pi} \left(\frac{4\pi^2 f^2 \text{FQ}}{c^2} \right)^2 \mathbb{E}[|H_0(f)|^2] \left[\frac{\text{W}}{\text{Hz}} \right]$ and the frequency-selective beamforming gain term be defined as

$$\mathcal{G}_{\text{DMA}}(\phi, f) = |\mathbf{f}_{\text{DMA}}^T(f) \mathbf{h}(\phi, f)|^2. \quad (13)$$

The received power spectral density is expressed in terms of the transmit power spectral density as

$$P_R(\phi, f) = \lim_{T_0 \rightarrow \infty} \frac{1}{T_0} \frac{\lambda^2}{4\pi} \mathbb{E}[S_r(f)] \quad (14)$$

$$= \left(\frac{\lambda}{4\pi r} \right)^2 P_T(f) \mathcal{G}_{\text{DMA}}(\phi, f) \left[\frac{\text{W}}{\text{Hz}} \right]. \quad (15)$$

The DMA configuration affects the receive signal power through the frequency-selective beamforming gain.

In this paper, we compare the DMA-based transmitter with a TTD architecture [5]. The TTD beamforming architecture for a conventional array with τ_n delay at n th element produces a frequency-selective beamforming vector as $\mathbf{f}_{\text{TTD}}(f) = [e^{j2\pi f \tau_1}, \dots, e^{j2\pi f \tau_N}]^T$ and the corresponding beamforming gain is $\mathcal{G}_{\text{TTD}}(\phi, f) = |\mathbf{f}_{\text{TTD}}^T(f) \mathbf{h}(\phi, f)|^2$ where the intrinsic phase vector is an all ones vector. Prior work has compared the frequency-selective beamforming gain of the TTD and phased-array but comparison with DMAs is missing [26]. We choose TTD as a benchmark for comparison. DMA beamforming is energy-efficient but is complicated by the coupled phase and magnitude constraint. In Section III, we discuss how to design the DMA beamformer despite these limitations.

C. Signal to noise ratio and achievable rate

We measure the system performance in terms of the achievable rate. Let k_B be the Boltzmann constant in J/K and T be the noise temperature of the antenna in K. The noise spectral density at the receiver is $N_0 = k_B T \left[\frac{\text{W}}{\text{Hz}} \right]$. The received SNR for a line-of-sight receiver at angle ϕ operating at frequency f is defined as $\text{SNR}(\phi, f) = \frac{P_R(\phi, f)}{N_0}$. The received SNR varies with frequency.

We model a communication system where the center frequency of the data transmission band can be dynamically reconfigured as the DMA has the ability to resonate at different frequencies. Let the communication bandwidth be fixed as B . Let the operating frequency allocated to the user by the transmitter be f_t which can be dynamically chosen from the range $[f_{t,\min}, f_{t,\max}]$. The DMA transmitter transfers data in the band $[f_t - \frac{B}{2}, f_t + \frac{B}{2}]$. In the data transmission band, we assume an OFDM system with K_d subcarriers. The achievable rate for a receiver with AoD as ϕ and operating frequency f_t is defined as

$$R(\phi, f_t) = \frac{B}{K_d} \sum_{k=1}^{K_d} \log_2(1 + \text{SNR}(\phi, f_k)) \text{ [bits/s]}. \quad (16)$$

In this work, we focus on the problem of configuring the resonant frequencies of the transmit DMA and choosing the operating frequency to maximize the frequency-selective beamforming gain at the receiver. Optimizing the beamforming gain will result in higher received SNR. Assuming equal power allocation across frequency, maximizing SNR is equivalent to maximizing achievable rate.

III. FREQUENCY-SELECTIVE BEAMFORMING GAIN OPTIMIZATION AND ANALYSIS

The main focus of this section is to find the DMA configuration that achieves the highest beamforming gain over a line-of-sight channel. The AoD is assumed to be perfectly known

in this section. We propose a method for AoD estimation in Section IV. We propose a two-stage optimization approach to maximize the gain at a specific AoD. In the first stage, we develop closed-form expressions for the DMA resonant frequencies to maximize the beamforming gain at a particular operating frequency and desired angle. Using the results of Section III-A, we propose a second-stage optimization over the operating frequency in Section III-B. The prior work on DMA beamforming is limited only to the first stage optimization [9], [10], which we show is sub-optimal compared to our two-stage optimization approach in the proposed wideband setting. Although the first stage optimization has been studied, our formulation differs from the prior work as we explicitly solve for the resonant frequency.

A. Beamforming gain optimization

We formulate the problem of maximizing the beamforming gain for a particular angle ϕ_{AoD} and operating frequency f_t in terms of the reconfigurable resonant frequency of each DMA element. We assume that the resonant frequencies can attain any positive real value $\{f_{r,n}\}_{n=1}^N$. We mathematically formulate the problem as follows:

$$\mathbf{P1} : \max_{\{f_{r,n}\}_{n=1}^N} \mathcal{G}_{\text{DMA}}(\phi_{\text{AoD}}, f_t), \quad (17a)$$

$$\text{s.t. } \{f_{r,n}\}_{n=1}^N > 0. \quad (17b)$$

To highlight why problem **P1** is challenging compared to the conventional TTD beamforming and to use some of the insights from the TTD solution to address the challenge in DMA beamforming, we present problem **P2** for maximizing $\mathcal{G}_{\text{TTD}}(\phi_{\text{AoD}}, f_t)$. For a TTD array, the mathematical formulation for maximizing the beamforming gain at angle ϕ_{AoD} and operating frequency f_t is

$$\mathbf{P2} : \max_{\{\tau_n\}_{n=1}^N} \mathcal{G}_{\text{TTD}}(\phi_{\text{AoD}}, f_t), \quad (18a)$$

$$\text{s.t. } \{\tau_n\}_{n=1}^N \geq 0. \quad (18b)$$

The optimal solution for **P2** is expressed in terms of ϕ_{AoD} as

$$\tau_n^* = \begin{cases} \frac{d_y}{c}(n-1)\sin(\phi_{\text{AoD}}), & \phi_{\text{AoD}} \geq 0, \\ \frac{d_y}{c}(n-N)\sin(\phi_{\text{AoD}}), & \phi_{\text{AoD}} < 0. \end{cases} \quad (19)$$

The maximum value of the beamforming gain is $\mathcal{G}_{\text{TTD}}^*(\phi_{\text{AoD}}, f_t) = N^2$.

For wideband transmission, the beam squint-effect leads to reduction in beamforming gain for frequencies away from the center frequency. This degradation in phased-array gain has been studied in comparison to TTD in prior work [26] but comparison with a DMA is missing. The DMA has higher frequency-selectivity compared to phased-array. With this solution in (19), the beam squint is eliminated completely for a line-of-sight channel, whereas for DMA this is not possible. The solution for **P2** is straightforward because the beamforming weight lies on a unit modulus circle, i.e., the magnitude for the beamforming weight is fixed. We use this observation to reformulate the objective in **P1**.

The optimization variable $f_{r,n}$ in **P1** appears in both the phase and magnitude of the DMA beamforming weight, which

makes it challenging to solve the problem directly in terms of the resonant frequencies $f_{r,n}$. In (9), we observe that the magnitude of $[\mathbf{f}_{\text{DMA}}(f)]_n$ is sinusoidal in terms of the phase angle $\psi_n(f) \in [-\pi, 0]$. In the complex domain, the locus of the beamforming weight $[\mathbf{f}_{\text{DMA}}(f)]_n$ is a circle with radius of 0.5 centered at $\frac{-j}{2}$. Compared to a phase-shifter or TTD weight with $\varphi_{r,n} \in [0, 2\pi)$, the DMA beamforming weight has a limited phase-range in $\psi_n(f) \in [-\pi, 0]$. To simplify the DMA beamforming constraint, we define a phase angle $\tilde{\psi}_n(f)$ which covers the whole angular range of 2π . We use a shift-of-origin transformation for the DMA beamforming weight as [9]

$$[\mathbf{f}_{\text{DMA}}(f)]_n = \frac{-j + e^{j\tilde{\psi}_n(f)}}{2}. \quad (20)$$

The relation between $\psi_n(f)$ and $\tilde{\psi}_n(f)$ is

$$\psi_n(f) = \frac{\tilde{\psi}_n(f)}{2} - \frac{\pi}{4}, \quad (21)$$

where $\tilde{\psi}_n(f) \in [-\frac{3\pi}{2}, \frac{\pi}{2}]$. In problem **P1**, the objective is to maximize the beamforming gain at f_t by optimizing the resonant frequencies $\{f_{r,n}\}_{n=1}^N$. Substituting $f = f_t$ in (2) and (21), we express the resonant frequency of the n th slot at operating frequency f_t as

$$f_{r,n} = \sqrt{f_t^2 + \frac{\Gamma f_t}{2\pi} \tan\left(\frac{\pi}{4} + \frac{\tilde{\psi}_n(f_t)}{2}\right)}. \quad (22)$$

The shift-of-origin transformation simplifies the beamforming gain optimization in **P1** by reformulating the problem in terms of $\tilde{\psi}_n(f)$ and then computing the optimal $f_{r,n}$ using (22).

A shift-of-origin transformation can also be applied to the DMA beamformer to define the unit-modulus DMA beamforming vector $\tilde{\mathbf{f}}_{\text{DMA}}(f)$ such that $[\tilde{\mathbf{f}}_{\text{DMA}}(f)]_n = e^{j\tilde{\psi}_n(f)}$. The original DMA beamforming vector is expressed in terms of $\tilde{\mathbf{f}}_{\text{DMA}}(f)$ as $\mathbf{f}_{\text{DMA}}(f) = \frac{-j\mathbf{1} + \tilde{\mathbf{f}}_{\text{DMA}}(f)}{2}$. The DMA beamforming gain in (13) is $\mathcal{G}_{\text{DMA}}(\phi_{\text{AoD}}, f) = \frac{1}{4} \left| -\mathbf{j}\mathbf{1}^T \mathbf{h}(\phi_{\text{AoD}}, f) + \tilde{\mathbf{f}}_{\text{DMA}}^T(f) \mathbf{h}(\phi_{\text{AoD}}, f) \right|^2$. We reformulate **P1** in terms of the unit-modulus beamforming weight as

$$\mathbf{P1a} : \max_{\{\tilde{\psi}_n(f_t)\}_{n=1}^N} \mathcal{G}_{\text{DMA}}(\phi_{\text{AoD}}, f_t), \quad (23a)$$

$$\text{s.t. } \{\tilde{\psi}_n(f_t)\}_{n=1}^N \in \left[-\frac{3\pi}{2}, \frac{\pi}{2} \right]. \quad (23b)$$

The closed-form expression for the optimal $\tilde{\psi}_n(f_t)$ and the expression for the maximum value of beamforming gain at ϕ_{AoD} and f_t are given in the following lemma.

Lemma 1: Let $\mathcal{S}(\phi, f_t) = \frac{\sin(\pi N \frac{f_t d_y (n_g + \sin(\phi))}{c})}{\sin(\pi \frac{f_t d_y (n_g + \sin(\phi))}{c})}$. The optimal solution to problem **P1a** $\{\tilde{\psi}_n^*(f_t)\}_{n=1}^N$ takes the form

$$\begin{aligned} \tilde{\psi}_n^*(f_t) &= -\frac{\pi}{2} \text{sgn}(\mathcal{S}(\phi_{\text{AoD}}, f_t)) \\ &+ \frac{2\pi f_t d_y (n_g + \sin(\phi_{\text{AoD}}))}{c} \left(n - 1 - \frac{N-1}{2} \right) + 2m\pi, \end{aligned} \quad (24)$$

where m is an integer such that $\tilde{\psi}_n^*(f_t) \in [-\frac{3\pi}{2}, \frac{\pi}{2}]$. The maximum value of the beamforming gain at ϕ_{AoD} and f_t is

$$\mathcal{G}_{\text{DMA}}^*(\phi_{\text{AoD}}, f_t) = \frac{1}{4} (N + |\mathcal{S}(\phi_{\text{AoD}}, f_t)|)^2. \quad (25)$$

Proof: We bound the beamforming gain from (23a) as

$$\begin{aligned} \mathcal{G}_{\text{DMA}}(\phi, f_t) &\stackrel{(a)}{\leq} 0.25 \left(\left| -\mathbf{j}\mathbf{1}^T \mathbf{h}(\phi, f_t) \right|^2 + \left| \tilde{\mathbf{f}}_{\text{DMA}}^T(f_t) \mathbf{h}(\phi, f_t) \right|^2 \right. \\ &\quad \left. + 2 \left| -\mathbf{j}\mathbf{1}^T \mathbf{h}(\phi, f_t) \right| \left| \tilde{\mathbf{f}}_{\text{DMA}}^T(f_t) \mathbf{h}(\phi, f_t) \right| \right). \end{aligned} \quad (26)$$

We simplify the term $-\mathbf{j}\mathbf{1}^T \mathbf{h}(\phi, f_t) = \mathcal{S}(\phi, f_t) e^{j(-\frac{\pi}{2} - \pi(N-1)\frac{f_t d_y (n_g + \sin(\phi))}{c})}$. Equating the phase of the terms $-\mathbf{j}\mathbf{1}^T \mathbf{h}(\phi, f_t)$ and $\tilde{\mathbf{f}}_{\text{DMA}}^T(f_t) \mathbf{h}(\phi, f_t)$, we obtain equality in (a) which proves the desired result. \square

From the expression in (24), we observe that the optimal phase can be decomposed into two terms — a term dependent on the slot index n and a term independent of n . The term independent of n is the constant phase rotation applied to each element to maximize the gain. The beamforming gain is not invariant to the common phase rotation because of the Lorentzian constraint. Our proposed solution resembles the optimal phase rotation approach discussed in the prior work [9]. We propose a closed-form solution that is applicable for a line-of-sight channel and for the ideal case with no waveguide attenuation unlike [9] which used a brute-force search approach to compute the optimal phase rotation in a setting with a non-ideal DMA.

The optimal resonant frequencies are computed by substituting the closed-form expression for $\tilde{\psi}_n^*(f_t)$ from (24) in (22). Let the optimal solution to problem **P1** be $\{f_{r,n}^*\}_{n=1}^N$. We express it in closed-form as

$$\begin{aligned} f_{r,n}^* &= \left(f_t^2 + \frac{\Gamma f_t}{2\pi} \tan \left(\frac{\pi}{4} (1 - \text{sgn}(\mathcal{S}(\phi_{\text{AoD}}, f_t))) \right) \right. \\ &\quad \left. + \frac{\pi f_t d_y (n_g + \sin(\phi_{\text{AoD}}))}{c} \left(n - 1 - \frac{N-1}{2} \right) \right)^{\frac{1}{2}}. \end{aligned} \quad (27)$$

We now have a mapping between the DMA resonant frequencies to the receiver angle as a parametric function of the operating frequency. For a fixed f_t , (27) is the optimal solution to configure the DMA. In Section III-B, we go one step further and optimize the communication system with a flexible choice of operating frequency that can leverage the DMA frequency reconfigurability to further improve the beamforming gain.

B. Optimizing operating frequency and angular coverage

The maximum value of $\mathcal{G}_{\text{DMA}}^*(\phi_{\text{AoD}}, f_t)$ varies with ϕ_{AoD} and f_t as proved in Lemma 1. For a TTD array, the maximum beamforming gain is independent of ϕ_{AoD} and f_t and equals N^2 . This begs the question whether it is possible to attain the maximum value of N^2 for a DMA too? For a DMA operating in a system with wider spectrum availability, we formulate a problem of optimally choosing the operating frequency to maximize the beamforming gain at a particular angle. We assume that the operating frequency range of the DMA is

$[f_{t,\min}, f_{t,\max}]$. Mathematically, **P1** can be modified to include the operating frequency optimization as follows:

$$\mathbf{P3} : \max_{f_t} \left(\max_{\{f_{r,n}\}_{n=1}^N} \mathcal{G}_{\text{DMA}}(\phi_{\text{AoD}}, f_t) \right), \quad (28a)$$

$$\text{s.t. } \{f_{r,n}\}_{n=1}^N > 0, \quad (28b)$$

$$f_t \in [f_{t,\min}, f_{t,\max}]. \quad (28c)$$

In the following lemma, we prove that it is possible to attain the same maximum value as that of a TTD array by optimizing over the operating frequency.

Lemma 2: Let $p_{\min} = \frac{f_{t,\min} d_y (n_g + \sin(\phi_{\text{AoD}}))}{c}$ and $p_{\max} = \frac{f_{t,\max} d_y (n_g + \sin(\phi_{\text{AoD}}))}{c}$. The optimal solution to problem **P3** f_t^* is expressed in closed-form as

$$f_t^*(\phi_{\text{AoD}}) = \frac{p^* c}{d_y (\sin(\phi_{\text{AoD}}) + n_g)}, \quad (29)$$

where $p^* \in [p_{\min}, p_{\max}]$ is the solution to the problem

$$p^* = \underset{p \in [p_{\min}, p_{\max}]}{\text{argmax}} \left| \frac{\sin(\pi N p)}{\sin(\pi p)} \right|. \quad (30)$$

The beamforming gain at ϕ_{AoD} is $\mathcal{G}_{\text{DMA}}^*(\phi_{\text{AoD}}, f_t^*(\phi_{\text{AoD}})) \leq N^2$, where equality holds when $\exists p^* \in \mathbb{N}$. At this maximum value, the optimal resonant frequencies of the DMA elements are $f_{r,n}^*(\phi_{\text{AoD}}) = f_t^*(\phi_{\text{AoD}}) \forall n$. For the case where $\nexists p^* \in \mathbb{N}$, the optimal resonant frequencies are obtained by solving (30) numerically and substituting $f_t^*(\phi_{\text{AoD}})$ in (27).

Proof: The inner maximization in problem **P3** is solved in Lemma 1 and the closed-form resonant frequency solution is expressed in (27). We leverage these solutions to solve problem **P3**. The optimal operating frequency is expressed as

$$f_t^*(\phi) = \underset{f_t \in [f_{t,\min}, f_{t,\max}]}{\text{argmax}} \mathcal{G}_{\text{DMA}}^*(\phi, f_t) = \underset{f_t \in [f_{t,\min}, f_{t,\max}]}{\text{argmax}} |\mathcal{S}(\phi, f_t)|. \quad (31)$$

There are two cases for expressing the solution of **P3** depending on whether p^* is a natural number or not.

Case 1: The global maximum of $|\mathcal{S}(\phi, f_t)|$ is N and is attained when $p^* = \frac{f_t^* d_y (n_g + \sin(\phi))}{c}$ is a natural number. Using (27), it can be easily verified that $f_{r,n}^*(\phi) = f_t^*(\phi)$ when p^* is a natural number.

Case 2: The global maximum N cannot be attained if there is no integer $p^* \in [p_{\min}, p_{\max}]$. Hence, p^* is obtained numerically by solving (30). \square

From Lemma 2, we see that the maximum possible DMA beamforming gain is N^2 only when p^* is a natural number. This maximum gain equals that of a TTD array but only at the optimal frequency. Lemma 2 also demonstrates that all slots should have the same optimal resonant frequency for the DMA to attain the maximum gain. The gain is less than N^2 when there does not exist any natural number in the range $[p_{\min}, p_{\max}]$. In this case, the optimal resonant frequencies are distinct for each DMA slot.

The DMA angular range for beamforming is limited by the constraint on the operating frequency in (28c). For the unconstrained DMA case, i.e., without constraint (28c), the maximum beamforming gain is N^2 for all AoDs. Imposing constraint (28c) limits the angular range for which the maximum gain N^2 is attainable. The limits p_{\min} and p_{\max} play

a critical role in defining the regime in which the maximum gain of N^2 can be attained. These limits depend on the DMA parameters like the refractive index n_g and the inter-antenna spacing d_y . This dependence motivates us to design n_g and d_y to improve the beamforming coverage.

We first define the maximum gain angular range of the DMA. The maximum gain angular range is the set of angles over which the DMA beamforming gain is N^2 for some frequency $f_t^*(\phi) \in [f_{t,\min}, f_{t,\max}]$. Let this set be denoted as Φ . Note that the frequency at which the maximum gain is achieved is dependent on the angle as proved in Lemma 2. We define the beamforming criterion as

$$\mathcal{G}_{\text{DMA}}^*(\phi, f_t^*(\phi)) = N^2 \forall \phi \in \Phi, f_t^*(\phi) \in [f_{t,\min}, f_{t,\max}]. \quad (32)$$

In other words, for each AoD $\phi \in \Phi$, we want to obtain the optimal operating frequency solution corresponding to the case when p^* is a natural number from Lemma 2. We provide the closed-form design solution for n_g^* and d_y^* to satisfy the beamforming criterion from (32) in the following lemma.

Lemma 3: For the set $\Phi = \{\phi_{\text{AoD}} : -\pi < \phi_{\text{lw}} \leq \phi_{\text{AoD}} \leq \phi_{\text{up}} < \pi\}$, the closed-form design solution for n_g^* that satisfies (32) is

$$n_g^* = \frac{\sin(\phi_{\text{up}}) - \sin(\phi_{\text{lw}})}{2} \left(\frac{f_{t,\max} + f_{t,\min}}{f_{t,\max} - f_{t,\min}} \right) - \frac{\sin(\phi_{\text{up}}) + \sin(\phi_{\text{lw}})}{2}, \quad (33)$$

and the closed-form design solution for d_y^* is

$$d_y^* = \frac{cp^*(f_{t,\max} - f_{t,\min})}{(\sin(\phi_{\text{up}}) - \sin(\phi_{\text{lw}}))f_{t,\min}f_{t,\max}}, \text{ where } p^* \in \mathbb{N}. \quad (34)$$

Proof: From **Case 1** of Lemma 2, we see that to satisfy the requirement $\mathcal{G}_{\text{DMA}}^*(\phi, f_t^*) = N^2$, the value of p^* has to be a natural number which lies inside $\left[\frac{f_{t,\min}d_y(n_g + \sin(\phi))}{c}, \frac{f_{t,\max}d_y(n_g + \sin(\phi))}{c} \right]$. To satisfy $\mathcal{G}_{\text{DMA}}^*(\phi, f_t^*) = N^2 \forall \phi \in [\phi_{\text{lw}}, \phi_{\text{up}}]$, the upper limit computed at $\phi \in [\phi_{\text{lw}}, \phi_{\text{up}}]$ should be greater than or equal to a natural number p^* and the lower limit computed at $\phi \in [\phi_{\text{lw}}, \phi_{\text{up}}]$ should be less than or equal to the same natural number p^* . Mathematically, $\forall \phi \in [\phi_{\text{lw}}, \phi_{\text{up}}]$, we get

$$\frac{f_{t,\min}d_y}{c}(n_g + \sin(\phi)) \leq p^* \leq \frac{f_{t,\max}d_y}{c}(n_g + \sin(\phi)). \quad (35)$$

Both the upper and lower limit on p^* are an increasing function of ϕ in the desired angular range. Hence, we have

$$\frac{f_{t,\min}d_y(n_g + \sin(\phi_{\text{up}}))}{c} \leq p^* \leq \frac{f_{t,\max}d_y(n_g + \sin(\phi_{\text{lw}}))}{c}. \quad (36)$$

By equating the upper and lower limit of p^* in (36), we get the desired results in (33) and (34) where equality holds for $n_g = n_g^*$ and $d_y = d_y^*$. \square

The beamforming criterion in (32) can be satisfied by an optimal design choice of the refractive index and element spacing for the DMA. For the special case of a symmetric angular range with ϕ_{max} as the maximum desired beamforming angle from broadside ($\phi_{\text{AoD}} = 0$), let $\phi_{\text{lw}} = -\phi_{\text{max}}$ and $\phi_{\text{up}} = \phi_{\text{max}}$. This leads to $n_g^* = \sin(\phi_{\text{max}}) \left(\frac{f_{t,\max} + f_{t,\min}}{f_{t,\max} - f_{t,\min}} \right)$ and

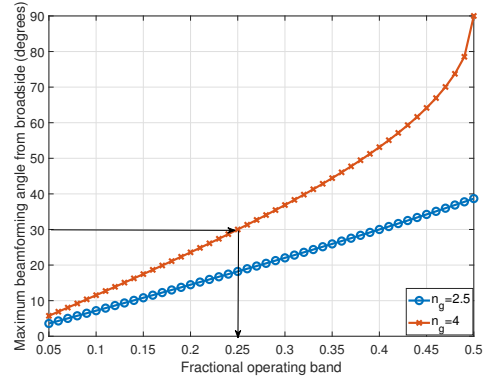


Fig. 2: The DMA maximum gain angular range from broadside is plotted as a function of the fractional operating band for different refractive indices. The maximum beamforming angle can be improved using wider operating band and higher refractive index.

$d_y^* = \frac{cp^*(f_{t,\max} - f_{t,\min})}{2\sin(\phi_{\text{max}})f_{t,\min}f_{t,\max}}$. From **Case 1** of Lemma 2, we see that the maximum value of beamforming gain N^2 is obtained when the value of p^* is chosen to be a natural number. As d_y^* depends on p^* , a reasonable choice of p^* should be made such that the spacing is not too large to avoid grating lobes and not too small to avoid mutual coupling between different elements.

The angular coverage is limited by the available choices of the waveguide substrate. Let n_g^{max} be the maximum practically feasible waveguide refractive index. This imposes the constraint

$$n_g^* = \sin(\phi_{\text{max}}) \left(\frac{f_{t,\max} + f_{t,\min}}{f_{t,\max} - f_{t,\min}} \right) \leq n_g^{\text{max}}. \quad (37)$$

Let the frequency range over which the DMA slots can be tuned be $T_r = f_{t,\max} - f_{t,\min}$. For a center frequency of the tuning range f_c , let $f_{t,\max} = f_c + \frac{T_r}{2}$ and $f_{t,\min} = f_c - \frac{T_r}{2}$. From (37), we compute ϕ_{max} as

$$\phi_{\text{max}} = \sin^{-1} \left(\frac{n_g^{\text{max}} T_r}{2f_c} \right). \quad (38)$$

From (38), we observe that to maximize the DMA beamforming angular coverage, the DMA should use the highest feasible waveguide refractive index and the maximum possible operating range T_r for the given f_c . In Fig. 2, we plot ϕ_{max} as a function of the fractional operating band $\frac{T_r}{f_c}$ for the cases $n_g = 2.5$ and $n_g = 4$. A typical base station serves a sector of 60° , i.e., $\phi_{\text{max}} = 30^\circ$. For this value of ϕ_{max} , the required fractional operating band is $\frac{T_r}{f_c} = 0.25$ for $n_g^{\text{max}} = 4$ as marked in Fig. 2. This design value of the refractive index is feasible. For example, Germanium has a refractive index of 4.

C. DMA beamforming gain frequency response analysis

So far, we have demonstrated how the DMA can achieve a gain of N^2 at AoD ϕ_{AoD} only at a particular frequency $f_t^*(\phi_{\text{AoD}})$. The data transmission, however, is for a specific bandwidth B . A phased-array experiences degradation in the beamforming gain for frequencies away from the center frequency due to beam-squint [26]. While DMA beamforming

also exhibits beam-squint, the DMA beamforming gain experiences further wideband losses because of the per-element frequency-selective Lorentzian response shown in (1).

We analyze the frequency response of the DMA at an AoD inside the desired angular range for a bandwidth around the optimal operating frequency. For a DMA designed using the refractive index and element spacing from Lemma 3, the maximum beamforming gain N^2 is attained at $f_t^*(\phi)$ for any AoD ϕ in the desired angular range $[\phi_{lw}, \phi_{up}]$. To attain the maximum beamforming gain, the resonant frequencies are tuned based on Lemma 2, i.e., $f_{r,n}^*(\phi) = f_t^*(\phi)$, $\forall n \in \{1, \dots, N\}$. Hence, we have $[\mathbf{f}_{\text{DMA}}(f)]_n = \frac{\Gamma f}{2\pi(f_t^*(\phi))^2 - 2\pi f^2 + j\Gamma f}$, $\forall n \in \{1, \dots, N\}$. Substituting $[\mathbf{f}_{\text{DMA}}(f)]_n$ in (13), we have

$$\mathcal{G}_{\text{DMA}}(\phi, f) = \left| \frac{\Gamma f}{2\pi(f_t^*(\phi))^2 - 2\pi f^2 + j\Gamma f} \right|^2 \left| \mathbf{1}^T \mathbf{h}(\phi, f) \right|^2. \quad (39)$$

To analyze the overall DMA beamforming response, we write $\mathcal{G}_{\text{DMA}}(\phi, f)$ as product of the per-element frequency response $\mathcal{G}_{\text{element}}(\phi, f) = \left| \frac{\Gamma f}{2\pi(f_t^*(\phi))^2 - 2\pi f^2 + j\Gamma f} \right|^2$ and the frequency response of the array of DMA slots $\mathcal{G}_{\text{array}}(\phi, f) = \left| \mathbf{1}^T \mathbf{h}(\phi, f) \right|^2$. We can verify that the maximum value of N^2 is attained at $f = f_t^*(\phi)$. For $f \neq f_t^*(\phi)$, the beamforming gain $\mathcal{G}_{\text{DMA}}(\phi, f) < N^2$ as $\mathcal{G}_{\text{element}}(\phi, f) < 1$ and $\mathcal{G}_{\text{array}}(\phi, f) < N^2$.

To analyze the DMA bandwidth for which the beamforming gain does not fall below a certain threshold of ν times the maximum, we define the ν cutoff frequencies. Let the upper ν cutoff frequency be the highest frequency for which $\mathcal{G}_{\text{DMA}}(\phi, f) \geq \nu N^2$ and be denoted as $f_{e,\nu}^u$. Let the lower ν cutoff frequency be the lowest frequency for which $\mathcal{G}_{\text{DMA}}(\phi, f) \geq \nu N^2$ and be denoted as $f_{e,\nu}^l$. Let us define the ν bandwidth as $B_\nu = f_{e,\nu}^u - f_{e,\nu}^l$. We first analyze the cutoff frequencies and bandwidth for $\mathcal{G}_{\text{element}}(\phi, f)$ in the following lemma. Let $f_{e,\nu}^u$, $f_{e,\nu}^l$, and $B_{e,\nu}$ be the upper cutoff frequency, lower cutoff frequency, and the bandwidth for the term $\mathcal{G}_{\text{element}}(\phi, f)$.

Lemma 4: Let $\rho(\nu) = \frac{\nu}{1-\nu}$. For $\mathcal{G}_{\text{element}}(\phi, f)$, the closed-form exact expression for the ν cutoff frequencies is

$$f_{e,\nu}^l = \sqrt{(f_t^*(\phi))^2 + \frac{\Gamma^2 - \sqrt{\Gamma^4 + 16\Gamma^2\pi^2(f_t^*(\phi))^2\rho(\nu)}}{8\pi^2\rho(\nu)}}, \quad (40a)$$

$$f_{e,\nu}^u = \sqrt{(f_t^*(\phi))^2 + \frac{\Gamma^2 + \sqrt{\Gamma^4 + 16\Gamma^2\pi^2(f_t^*(\phi))^2\rho(\nu)}}{8\pi^2\rho(\nu)}}. \quad (40b)$$

The ν bandwidth for $\mathcal{G}_{\text{element}}(\phi, f)$ is expressed as

$$B_{e,\nu} = \frac{\Gamma}{2\pi\sqrt{\rho(\nu)}} + \mathcal{O}(\Gamma^3). \quad (41)$$

Proof: Mathematically, the closed-form expression for the ν cutoff frequencies are obtained as a solution to $\frac{\Gamma^2 f^2}{(2\pi(f_t^*(\phi))^2 - 2\pi f^2 + \Gamma^2 f^2)} = \nu$. We express this equation as a quadratic in f^2 . Solving the quadratic, we obtain the desired cutoff frequencies in (40a) and (40b). The ν bandwidth closed-form expression in (41) is obtained by applying binomial expansion to (40a) and (40b). \square

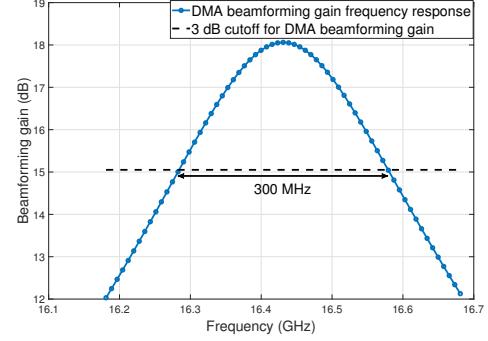


Fig. 3: The beamforming gain of the DMA configured to maximize gain at $\phi = -18^\circ$ and $f_t^*(-18^\circ) = 16.43$ GHz is shown as a function of frequency. The gain decreases for frequencies away from the optimal operating frequency. The 3 dB bandwidth of the beamforming gain frequency response is proportional to the damping factor.

The frequency response of $\mathcal{G}_{\text{element}}(\phi, f)$ has sharp degradation with frequency compared to $\mathcal{G}_{\text{array}}(\phi, f)$. Hence, we use the result from Lemma 4 directly to obtain $f_\nu^l \approx f_{e,\nu}^l$, $f_\nu^u \approx f_{e,\nu}^u$, and $B_\nu \approx B_{e,\nu}$. The key design insight is that the ν bandwidth B_ν is directly proportional to the DMA damping factor Γ . For example, for 3 dB bandwidth, i.e., $\nu = 0.5$, we have $\rho(0.5) = 1$ and $B_{0.5} \approx \frac{\Gamma}{2\pi}$.

D. Numerical results for DMA beamforming gain

We verify the closed-form expressions from Lemma 4 through numerical simulations. Let the number of elements on the DMA be $N = 8$. Let the center frequency of the DMA operating band be $f_c = 15$ GHz and the center wavelength $\lambda_c = \frac{c}{f_c}$. Let the DMA operating range be $f_{t,\min} = 12$ GHz and $f_{t,\max} = 18$ GHz, and let the desired angular range be $[-30^\circ, 30^\circ]$. From Lemma 3, we have the optimal spacing as $d_y^* = 0.42\lambda_c$ and the optimal refractive index $n_g^* = 2.5$. The angular direction is set to $\phi = -18^\circ$, which lies inside the desired angular range $[-30^\circ, 30^\circ]$. Let $\Gamma = \frac{2\pi f_c}{50}$. To maximize the beamforming gain at ϕ , we set the operating frequency and the DMA resonant frequencies using the expression in Lemma 2 with choice of $p^* = 1$. Using these parameters, we obtain the operating frequency $f_t^*(-18^\circ) = 16.43$ GHz from (29). In Fig. 3, we plot the frequency response of the DMA beamforming gain at $\phi = -18^\circ$. As expected, the DMA beamforming gain frequency response curves peaks at the operating frequency 16.43 GHz. From Fig. 3, the 3 dB bandwidth equals 300 MHz which validates Lemma 4.

We compare our proposed optimal operating frequency approach with methods used in the prior work.

1) *Fixed operating frequency approach:* Prior work on DMA beamforming is based on optimizing the beamforming gain for a specific AoD and fixed operating frequency [9]. Let the operating frequency be fixed to the center frequency f_c . The DMA resonant frequencies are configured using the closed-form expression in (27) where $f_t = f_c$. In Fig. 4, we plot the optimal DMA beamforming gain at f_c as a function of the angle ϕ , mathematically denoted as $\mathcal{G}_{\text{DMA}}^*(\phi, f_c)$ and computed using (25). We observe that $\mathcal{G}_{\text{DMA}}^*(\phi, f_c) \leq$

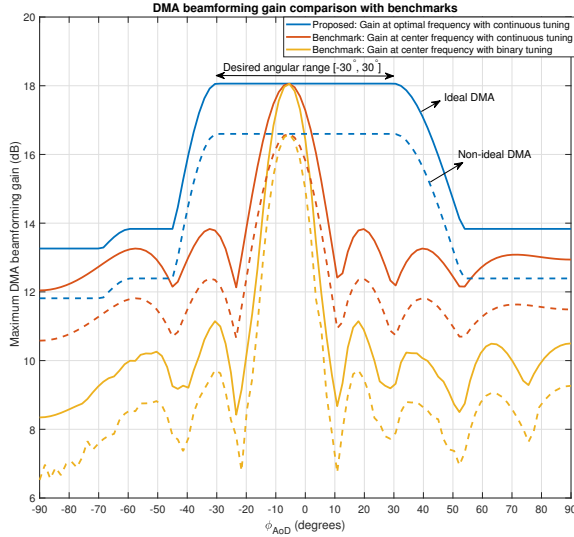


Fig. 4: The DMA beamforming gain as a function of the AoD is shown for both ideal and non-ideal DMA for different benchmarks. The proposed approach outperforms the benchmarks with a fixed operating frequency for all angles. Beyond $\pm 30^\circ$, the beamforming gain decreases because of the operating frequency constraint (28c).

$\mathcal{G}_{\text{DMA}}^*(\phi, f_t^*(\phi))$, $\forall \phi$. The equality holds only for a single angle denoted as ϕ_c such that $f_t^*(\phi_c) = f_c$. Mathematically, it is expressed as

$$\phi_c = \sin^{-1} \left(\frac{c}{f_c d_y} - n_g \right). \quad (42)$$

In Fig. 4, we use the simulation parameters same as in Fig. 3. In this case, (42) evaluates to $\phi_c = -5.74^\circ$. In Fig. 4, we see that $\mathcal{G}_{\text{DMA}}^*(\phi_c, f_c) = N^2$. For all angles $\phi \neq \phi_c$, we see that $\mathcal{G}_{\text{DMA}}^*(\phi, f_c) < N^2$. In Fig. 5, we plot the optimal frequency $f_t^*(\phi)$ from (29) as function of ϕ . By optimally choosing the operating frequency based on the angle as shown in Fig. 5, we significantly outperform the fixed operating frequency approach as indicated in Fig. 4 which shows a gain of N^2 in the desired angular range.

The maximum gain angular range depends on the DMA upper and lower tuning frequency limits. As $f_{t,\min} = 12$ GHz and $f_{t,\max} = 18$ GHz, the maximum beamforming angle for $n_g = 2.5$ is $\pm 30^\circ$. Beyond $\pm 30^\circ$, we observe a clipping in the optimal operating frequency curve in Fig. 5 to satisfy the operating frequency constraint (28c). This also reflects in the beamforming gain plot in Fig. 4, where we observe a decrease in the beamforming gain outside $\pm 30^\circ$. Without the DMA constraint (28c), the beamforming gain will be N^2 for the whole angular range. This is practically infeasible as the DMA would need to operated over a very wide frequency range of 10 GHz to 24 GHz. This is demonstrated in Fig. 5, where the monotonic curve extends beyond the feasible frequency range.

2) Comparison between binary and continuous weights:

In the analysis so far, we have assumed that DMA resonant frequencies are tunable to a continuous frequency value. Another option for configuring the DMA elements is a binary tuning mechanism leveraging PIN diodes instead of varactor

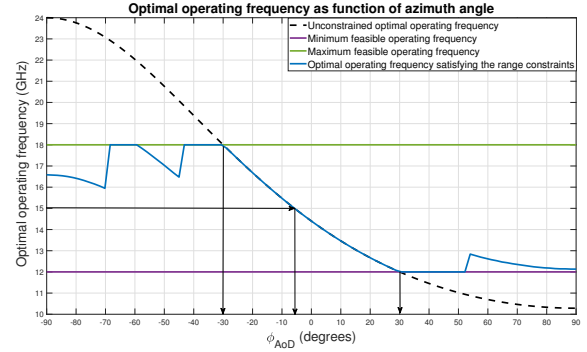


Fig. 5: The optimal operating frequency from our proposed approach is shown as a function of the AoD. A monotonic behavior for the desired angular range $\pm 30^\circ$ is observed which corresponds to the maximum gain in Fig. 4.

diodes [27]. PIN diodes can be used as RF switches with on and off states, as opposed to the continuous varactor diode tuning. While the PIN diode devices themselves consume more power than passive varactor diodes, varactor-based DMAs require high-resolution DACs for continuous tuning and can potentially consume more power than a PIN diode-based DMA system [28], [29]. Moreover, prior signal processing work on DMAs has highlighted the ability of binary tuning strategies to closely approach the performance of a continuous tuning strategy in narrowband settings [11], [12], [17]. The binary weight beamforming problem is formulated as

$$\mathbf{P4} : \max_{\mathbf{f}_{\text{DMA}}(f_c)} \mathcal{G}_{\text{DMA}}(\phi, f_c), \quad (43a)$$

$$\text{s.t. } [\mathbf{f}_{\text{DMA}}(f_c)]_n \in \{0, 1\}. \quad (43b)$$

We solve **P4** by maximizing over the set of feasible beamforming vectors by brute force search. The optimal beamforming gain at the center frequency obtained after solving **P4** is shown in Fig. 4. We see that when $\phi = \phi_c$, the DMA beamforming gain for binary and continuous weights are equal to the theoretical maximum N^2 . This observation is consistent with the result from Lemma 2 that at the optimal operating frequency, the resonant frequencies on all elements are same as the operating frequency. For all angles $\phi \neq \phi_c$, we see that the beamforming gain from binary weights is decreased compared to the continuous DMA beamforming weights. For angles outside $[-14^\circ, 2^\circ]$, the decrease is higher than 2 dB. This is because some of the antenna elements have beamforming weight as zero, i.e., they do not radiate, which reduces the effective number of antennas and hence the beamforming gain.

3) *Non-ideal DMA:* In the simulations so far, we have ignored the attenuation within the waveguide. For a practical DMA, the waveguide attenuation can degrade the beamforming gain [2]. To analyze the impact of waveguide attenuation, we denote the attenuation factor as α and assume an exponentially decaying attenuation vector as $\mathbf{g}(f) = [1, e^{-\alpha d_y}, \dots, e^{-\alpha(N-1)d_y}]^T$. The effective propagation channel is modified as $\mathbf{h}(\phi, f) = \mathbf{h}_{\text{dma}}(f) \odot \mathbf{a}(\phi, f) \odot \mathbf{g}(f)$. For simulations, we use $\alpha = 6$ [4] and use the resonant frequency solution corresponding to the ideal DMA case. In Fig. 4, we compare the beamforming gain of the ideal DMA

and the non-ideal DMA. We see that the non-ideal DMA with attenuation exhibits a slight degradation in the beamforming gain compared to the ideal DMA without attenuation. We also see that the proposed optimal frequency approach outperforms the benchmark fixed frequency approach for the non-ideal DMA too. Although inclusion of attenuation in the model leads to beamforming gain degradation, the overall comparison trend remains the same. Hence, we continue with the use of the ideal DMA model for subsequent analysis.

IV. SINGLE-SHOT BEAM TRAINING WITH DMAS

The analysis in Section III assumes that the transmitter knows the AoD ϕ . In practice, the transmitter performs beam training prior to data transmission to determine the beamforming vector based on AoD estimation. In conventional exhaustive search beam training, the beamforming vector is determined by sequentially configuring the array for different AoDs and choosing the angle with the highest beamforming gain to compute the optimal beamforming vector for the desired user. This process is inefficient for large arrays because the number of time slots required to perform beam training increases with the number of antennas [30]. In this section, we leverage the frequency reconfigurability of the DMA and propose a beam training procedure that estimates the optimal DMA configuration in a single time-slot.

A. System model for an array of DMAs

Let an array of N_z DMAs be arranged in the yz plane as shown in Fig. 6, where each DMA has N_y radiating slots. We assume that each DMA has the same intrinsic phase-shift. For a receiver on the xy plane, the effective propagation far-field channel for the array of DMAs is denoted as $\mathbf{h}_A(\phi, f) \in \mathbb{C}^{N_z N_y \times 1}$ and expressed in terms of $\mathbf{h}(\phi, f) \in \mathbb{C}^{N_y \times 1}$ as

$$\mathbf{h}_A(\phi, f) = \underbrace{[\mathbf{h}^T(\phi, f), \mathbf{h}^T(\phi, f), \dots, \mathbf{h}^T(\phi, f)]^T}_{N_z \text{ times}}. \quad (44)$$

As the elevation angle $\theta = 90^\circ$, the propagation channel from each DMA to the receiver in xy plane is the same. The extension to do beam training in both azimuth and elevation directions is a topic of future study.

The beamforming vector for the m th DMA in the array is denoted as $\mathbf{f}_{\text{DMA},m}(f)$. The beamforming vector for the array of DMAs is denoted as $\mathbf{f}_{\text{ADMA}}(f)$ and expressed as $\mathbf{f}_{\text{ADMA}}(f) = [\mathbf{f}_{\text{DMA},1}^T(f), \mathbf{f}_{\text{DMA},2}^T(f), \dots, \mathbf{f}_{\text{DMA},N_z}^T(f)]^T$. We assume that the same signal is input to each DMA and is represented by $H_0(f)$ at the waveguide input. Hence, the far-field component of the electric field is expressed similar to the single DMA expression from (10) as

$$\mathbf{E}_\phi(f) = \frac{\eta_0}{4\pi r} \left(\frac{2\pi f}{c} \right)^2 H_0(f) \mathbf{F} \mathbf{Q} \mathbf{f}_{\text{ADMA}}^T(f) \mathbf{h}_A(\phi, f) \left[\frac{\text{V/m}}{\text{Hz}} \right]. \quad (45)$$

The frequency-selective beamforming gain for the DMA array is defined similar to that of a single DMA as

$$\mathcal{G}_{\text{ADMA}}(\phi, f) = \left| \mathbf{f}_{\text{ADMA}}^T(f) \mathbf{h}_A(\phi, f) \right|^2 = \left| \sum_{m=1}^{N_z} \mathbf{f}_{\text{DMA},m}^T(f) \mathbf{h}(\phi, f) \right|^2. \quad (46)$$

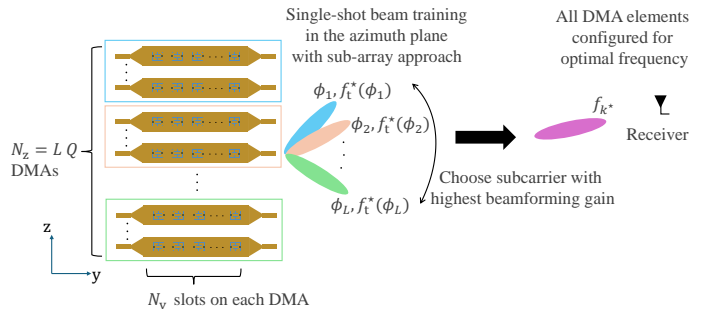


Fig. 6: An array of N_z DMAs where each DMA has N_y radiating slots. The sub-array approach enables simultaneous probing of different resonant frequencies using different frequencies to estimate the optimal resonant frequency. Post beam training, all elements of the DMA array are configured for the optimal frequency.

Similarly, the received power spectral density is $P_R(\phi, f) = \left(\frac{\lambda}{4\pi r} \right)^2 P_T(f) \mathcal{G}_{\text{ADMA}}(\phi, f) \left[\frac{\text{W}}{\text{Hz}} \right]$.

Let the resonant frequency of the n th element on the m th DMA in the array be denoted as $f_{r,n,m}$. Similar to the analysis in Section III, the maximum beamforming gain $\mathcal{G}_{\text{ADMA}}^*(\phi, f_t^*(\phi)) = N_z^2 N_y^2$ at a specific angle ϕ is attained when resonant frequencies of all elements on all DMAs are set to the optimal operating frequency $f_{r,n,m} = f_t^*(\phi)$. In practice, this optimal resonant frequency needs to be estimated using the beam training procedure as the AoD is unknown. We discuss the beam training procedure to estimate the optimal resonant frequency for the DMA.

B. Beam training with a single OFDM symbol

The goal of beam training is to estimate the optimal resonant frequency configuration for the DMA array to serve a user in a specific direction. To avoid training overhead, we propose a single-shot beam training procedure which enables probing different angular directions simultaneously with a single OFDM symbol by leveraging the frequency reconfigurability of the DMA. To achieve this goal, we use the sub-array approach for beam training. Let the array of N_z DMAs be grouped into L sub-groups where each sub-group has $Q = \frac{N_z}{L}$ DMAs as shown in Fig. 6. We assume that the angle ϕ lies inside the angular range $[-\phi_{\max}, \phi_{\max}]$. We divide this angular range into L sectors where the ℓ th sector has its peak gain at angle ϕ_ℓ . The DMA array is configured such that the ℓ th DMA sub-group focuses at ϕ_ℓ at the corresponding optimal frequency $f_t^*(\phi_\ell)$. The DMA resonant frequencies for beam training are configured as

$$f_{r,n,m} = f_t^*(\phi_\ell), \quad \forall n, m \in \{Q(\ell-1)+1, \dots, Q\ell\}. \quad (47)$$

This approach enables scanning different angles simultaneously with a single OFDM signal.

The DMA array transmits an OFDM pilot signal with K_{tr} subcarriers for beam training. Let the k th subcarrier frequency be f_k . The DMA beamforming vector configured according to (47) has the response $\mathbf{f}_{\text{ADMA}}(f_k)$ for the k th subcarrier. Let the actual AoD be ϕ . The beamforming gain at the receiver

at the k th subcarrier is $\mathcal{G}_{\text{ADMA}}(\phi, f_k)$. The receiver computes the subcarrier index with the highest beamforming gain as

$$k^* = \underset{k}{\operatorname{argmax}} \mathcal{G}_{\text{ADMA}}(\phi, f_k). \quad (48)$$

It sends feedback of the optimal subcarrier index to the transmit array. For the data transmission stage, the transmit DMA array is configured to operate for a specific bandwidth B centered around f_{k^*} . All DMA resonant frequencies are set to $f_{r,n,m} = f_{k^*}$. With this configuration, the maximum beamforming gain of $N_z^2 N_y^2$ is attained at f_{k^*} and $\hat{\phi}$ where $\hat{\phi} = \sin^{-1} \left(\frac{c}{d_y f_{k^*}} - n_g \right)$.

C. Beam training codebook design

In this section, we propose a codebook for the single-shot beam training approach. We first analyze the performance loss in beamforming when DMA resonant frequencies are set based on the subcarrier index obtained from the training procedure by simplifying $\mathcal{G}_{\text{ADMA}}(\phi, f_{k^*})$ as

$$\mathcal{G}_{\text{ADMA}}(\phi, f_{k^*}) = N_z^2 \left(\frac{\sin \left(\pi N_y \frac{(n_g^* + \sin(\phi))}{(n_g^* + \sin(\hat{\phi}))} \right)}{\sin \left(\pi \frac{(n_g^* + \sin(\phi))}{(n_g^* + \sin(\hat{\phi}))} \right)} \right)^2. \quad (49)$$

From (49), we see that the maximum beamforming gain of $N_z^2 N_y^2$ is attained when $\hat{\phi} = \phi$. As the error between the actual and estimated angle increases, the beamforming gain depreciates. In the following lemma, we quantify the allowable range of angle estimates for which the beamforming gain is above a certain threshold of δ times the maximum gain. Let $\Psi = \frac{(n_g^* + \sin(\phi))}{(n_g^* + \sin(\hat{\phi}))}$. The maximum value of $\left(\frac{\sin(\pi N_y \Psi)}{\sin(\pi \Psi)} \right)^2$ is N_y^2 . We define $\Psi_\delta(N_y)$ such that for $\Psi \in [-\Psi_\delta(N_y), \Psi_\delta(N_y)]$, the term $\left(\frac{\sin(\pi N_y \Psi)}{\sin(\pi \Psi)} \right)^2 \geq \delta N_y^2$ for $\delta < 1$. We can compute $\Psi_\delta(N_y)$ numerically. For example, for $\delta = 0.5$ (3 dB from maximum), we have $\Psi_\delta(N_y) \approx \frac{0.448}{N_y}$.

Lemma 5: The inequality $\mathcal{G}_{\text{ADMA}}(\phi, f_{k^*}) \geq \delta N_y^2 N_z^2$, is satisfied when the angle estimate $\hat{\phi}$ is bounded as follows.

$$\hat{\phi} \in \left[\sin^{-1} \left(\frac{n_g^* + \sin(\phi)}{1 + \Psi_\delta(N_y)} - n_g^* \right), \sin^{-1} \left(\frac{n_g^* + \sin(\phi)}{1 - \Psi_\delta(N_y)} - n_g^* \right) \right]. \quad (50)$$

Proof: When $\hat{\phi} = \phi$, we have $\Psi = 1$. To satisfy the gain threshold, we have $1 - \Psi_\delta(N_y) \leq \frac{(n_g^* + \sin(\phi))}{(n_g^* + \sin(\hat{\phi}))} \leq 1 + \Psi_\delta(N_y)$. Simplifying, we obtain the bounds on $\hat{\phi}$ in (50). \square

Beam codebook design: The goal of beam codebook design is to choose the angles where peak gain occurs for the L sectors in the beam training procedure to ensure that the beamforming gain $\mathcal{G}_{\text{ADMA}}(\phi, f_{k^*})$ for any ϕ in the desired range does not drop below a certain threshold of δ from the peak gain. We use the result from Lemma 5 to design the beam codebook. For the ℓ th sector, let ϕ_ℓ be the angle with the peak gain, i.e., $\mathcal{G}_{\text{ADMA}}(\phi_\ell, f_{k^*}) = N_y^2 N_z^2 \forall \ell = 1, \dots, L$. The main objective of the beam codebook design is to ensure that the beamforming gain for all angles in the range $[-\phi_{\max}, \phi_{\max}]$ is above $\delta N_y^2 N_z^2$. The peak angle of the first sector is designed

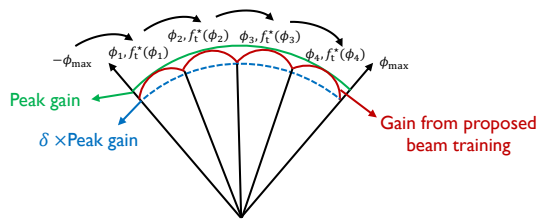
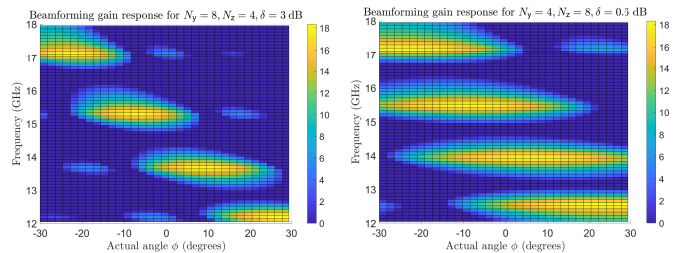


Fig. 7: The proposed beam codebook design ensures that the beamforming gain for all angles in the desired range is within a factor of δ from the maximum where δ is a design parameter.



(a) Beam training with $N_y = 8$, $N_z = 4$, $\delta = 3$ dB **(b)** Beam training with $N_y = 4$, $N_z = 8$, $\delta = 0.6$ dB

Fig. 8: The optimal operating frequency decreases in $L = 4$ steps as a function of the actual angle similar to the monotonic decreasing trend obtained for the continuous curve in Fig. 5. For the same L , the angular beam width is narrower for $N_y = 8$ compared to $N_y = 4$.

such that the gain at $-\phi_{\max}$ is $\delta N_y^2 N_z^2$. Equating the lower limit of $\hat{\phi}$ when $\phi = \phi_1$ in (50) to $-\phi_{\max}$, we obtain the expression of ϕ_1 as

$$\phi_1 = \sin^{-1} \left((\sin(-\phi_{\max}) + n_g^*) (1 + \Psi_\delta(N_y)) - n_g^* \right). \quad (51)$$

For the remaining sectors, we equate the lower limit of $\hat{\phi}$ when $\phi = \phi_\ell$ to the upper limit when $\phi = \phi_{\ell-1}$. With this procedure, the remaining $L - 1$ angles are obtained sequentially as

$$\phi_\ell = \sin^{-1} \left(\left(\sin(\phi_{\ell-1}) + n_g^* \right) \frac{(1 + \Psi_\delta(N_y))}{(1 - \Psi_\delta(N_y))} - n_g^* \right), \forall \ell > 1. \quad (52)$$

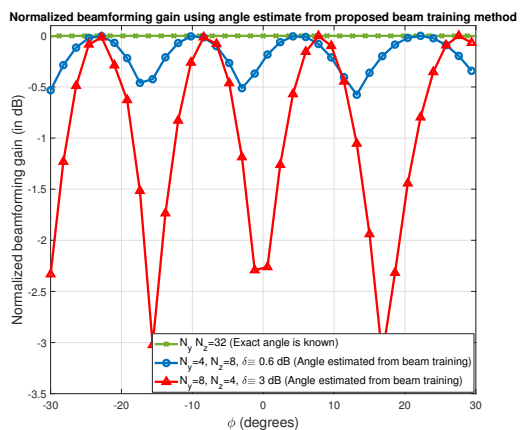


Fig. 9: Beamforming gain at the optimal operating frequency obtained using angle estimate depends on N_y and N_z whereas beamforming gain with perfect angle depends solely on the product $N_y N_z$.

The illustration of the beam codebook design procedure is shown in Fig. 7. To compare differences in the arrangement of elements on the DMA, and the impact on beam training, we describe two example cases when $\phi_{\max} = 30^\circ$ and $n_g^* = 2.5$ as follows:

- For $N_y = 8$, $N_z = 4$, $\delta \equiv 3$ dB, we have $\phi_1 = -22.83^\circ$, $\phi_2 = -7.9^\circ$, $\phi_3 = 8.21^\circ$, $\phi_4 = 27.16^\circ$.
- For $N_y = 4$, $N_z = 8$, $\delta \equiv 0.6$ dB, we have $\phi_1 = -23.33^\circ$, $\phi_2 = -9.51^\circ$, $\phi_3 = 5.22^\circ$, $\phi_4 = 22.04^\circ$.

The DMA resonant frequencies are set using (47). The beamforming gain response as a function of frequency and angle for these two cases is shown in Fig. 8a and Fig. 8b. The optimal subcarrier index at the receiver is computed using (48). Using the optimal resonant configuration, we evaluate (49) and plot the normalized beamforming gain at the optimal operating frequency as a function of the actual angle in Fig. 9. From the plot, we verify that the beamforming gain variation is within the desired threshold. This validates the result in Lemma 5. Using only four distinct values of resonant frequencies, it is possible to configure the DMA array such that the beamforming gain is within a certain threshold of the theoretical maximum obtained with perfect knowledge of the AoD. It suffices to use a DMA architecture with varactor diodes having the ability to be tuned to four distinct states instead of a continuous high resolution tunability.

V. ACHIEVABLE RATE RESULTS

We evaluate the achievable rate performance of the DMA array using the results from Section III and Section IV. In our proposed approach, the center frequency f_t is dynamically reconfigured depending on the AoD. We assume two cases for comparison: **Case 1-** When the AoD is perfectly known, the center frequency is set using Lemma 2; **Case 2-** When the AoD is unknown, we use the single-shot beam training procedure from Section IV and set $f_t = f_{k^*}$ obtained from (48). We also compare these two cases from our proposed approach to that of the benchmark DMA approach based on a fixed operating frequency. For the benchmark case, we set $f_t = f_c$ which is the center frequency of the DMA feasible operating frequency range. To compare with TTD, we also plot the achievable rate for TTD in Fig. 10.

For Fig. 10, we set $P = 250$ mW, $r = 500$ m, $n_g = 2.5$, $f_c = 15$ GHz, $d_y = 0.42\lambda_c$, $\Gamma = \frac{2\pi f_c}{50}$, $N_y = 8$, $N_z = 4$, and $T_r = 6$ GHz. For beam training, we use $L = 4$ and the angles with peak gain for each sector are chosen corresponding to the threshold $\delta \equiv 3$ dB. In Fig. 10, we plot the achievable rate averaged over angles $\phi \sim \mathcal{U}(-30^\circ, 30^\circ)$. In the OFDM system, we have $K_d = 64$ subcarriers. On the x axis of Fig. 10, we vary the communication bandwidth B. We observe that the achievable rate of the DMA configured based on our proposed optimal operating frequency approach outperforms the benchmark approach based on the fixed operating frequency. We also observe that the rate performance of the DMA when resonant frequencies are configured based on the single-shot beam training procedure is comparable to the rate obtained using perfect knowledge of the AoD. This validates the efficacy of the proposed single-shot beam training

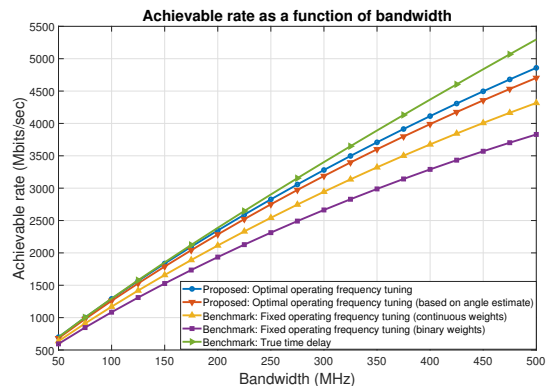


Fig. 10: The achievable rate DMA performance is comparable to the TTD performance up to a bandwidth of 300 MHz which is also the 3 dB DMA bandwidth as shown in Fig. 3.

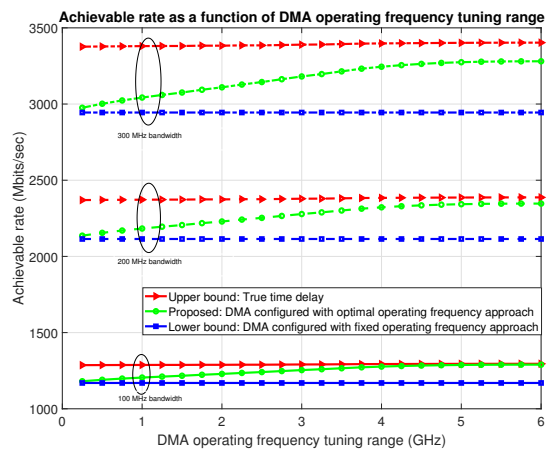


Fig. 11: DMA achievable rate based on optimal operating frequency approach is lower bounded by the DMA rate based on fixed frequency and upper bounded by the TTD rate for all tuning ranges.

approach. We also showed in Fig. 9 that with $L = 4$ sectors, the beamforming gain varies within 3 dB of the maximum. Hence, using only four resonant frequency configurations, it is possible to do both beam training and beamforming. In Fig. 10, we see that the achievable rate increases with bandwidth. The DMA achievable rate is comparable to that of TTD up to a bandwidth of 300 MHz (DMA 3 dB bandwidth) beyond which the performance gap increases. This is because of the DMA beamforming gain frequency-selectivity as shown in Fig. 3.

In Fig. 10, we assumed that the DMA operating range T_r is 6 GHz. In practice, this range depends on the reconfigurability of the DMA. In Fig. 11, we vary T_r by keeping all parameters same as Fig. 10 and plot the achievable rate obtained with three different values of the bandwidth B. The baseline approach performance does not change with T_r as the DMA operating frequency is always fixed to f_c . We observe that the proposed approach of dynamically configuring the DMA operating frequency outperforms the baseline fixed operating frequency approach for all tuning ranges. As T_r increases, the DMA achievable rate from the proposed approach tends to the TTD rate which acts as an upper bound. This implies that a DMA

with high tuning range can be an alternative to the power hungry TTD architecture.

VI. CONCLUSION AND FUTURE WORK

In this paper, we proposed a novel approach where the system configures the DMA resonant frequencies by optimally choosing the operating frequency based on the AoD. We derived a closed-form expression for the beamforming gain frequency response obtained using our proposed approach. We also developed a single-shot beam training approach for the DMA to estimate the optimal resonant frequency configuration. This approach gives comparable achievable rate performance with that obtained using perfect knowledge of the AoD. Our approach for configuring the DMA outperforms the benchmark fixed operating frequency approach for all tuning ranges. For future work, we plan to investigate the performance of the proposed approach in more practical settings like multipath wireless channel, incorporating mutual coupling between elements [31], and impedance matching impairments [32]. We also plan to extend the DMA beamforming approach to a multi-user scenario where reconfigurability of DMAs can be used for interference cancellation.

REFERENCES

- [1] N. Shlezinger, G. C. Alexandropoulos, M. F. Imani, Y. C. Eldar, and D. R. Smith, "Dynamic metasurface antennas for 6G extreme massive MIMO communications," *IEEE Wireless Commun.*, vol. 28, no. 2, pp. 106–113, 2021.
- [2] J. Carlson, N. V. Deshpande, M. R. Castellanos, and R. W. Heath Jr, "Wideband dynamic metasurface antenna performance with practical design impairments," *submitted to IEEE Trans. Wireless. Commun.*, Nov 2024.
- [3] M. Boyarsky, T. Sleasman, M. F. Imani, J. N. Gollub, and D. R. Smith, "Electronically steered metasurface antenna," *Scientific reports*, vol. 11, no. 1, p. 4693, 2021.
- [4] D. R. Smith, O. Yurduseven, L. P. Mancera, P. Bowen, and N. B. Kundtz, "Analysis of a waveguide-fed metasurface antenna," *Physical Review Applied*, vol. 8, no. 5, p. 054048, 2017.
- [5] N. V. Deshpande, M. R. Castellanos, and R. W. Heath Jr., "Nonuniform true time delay precoding in wideband MISO systems," in *Proc. 56th Asilomar Conf. Signals, Syst., Comput.*, 2022, pp. 1–5.
- [6] L. Dai, J. Tan, Z. Chen, and H. V. Poor, "Delay-phase precoding for wideband THz massive MIMO," *IEEE Trans. Wireless. Commun.*, vol. 21, no. 9, pp. 7271–7286, 2022.
- [7] R. Rotman, M. Tur, and L. Yaron, "True time delay in phased arrays," *Proc. IEEE*, vol. 104, no. 3, pp. 504–518, Mar. 2016.
- [8] H. Zhang, N. Shlezinger, F. Guidi, D. Dardari, M. F. Imani, and Y. C. Eldar, "Beam focusing for multi-user MIMO communications with dynamic metasurface antennas," in *ICASSP 2021 - 2021 IEEE International Conference on Acoustics, Speech and Signal Processing (ICASSP)*, 2021, pp. 4780–4784.
- [9] J. Carlson, M. R. Castellanos, and R. W. Heath, "Hierarchical codebook design with dynamic metasurface antennas for energy-efficient arrays," *IEEE Trans. Wireless. Commun.*, vol. 23, no. 10, pp. 14 790–14 804, 2024.
- [10] S. F. Kimaryo and K. Lee, "Downlink beamforming for dynamic metasurface antennas," *IEEE Trans. Wireless. Commun.*, vol. 22, no. 7, pp. 4745–4755, 2023.
- [11] N. Shlezinger, O. Dicker, Y. C. Eldar, I. Yoo, M. F. Imani, and D. R. Smith, "Dynamic metasurface antennas for uplink massive MIMO systems," *IEEE Trans. Commun.*, vol. 67, no. 10, pp. 6829–6843, July 2019.
- [12] L. You, J. Xu, G. C. Alexandropoulos, J. Wang, W. Wang, and X. Gao, "Energy efficiency maximization of massive MIMO communications with dynamic metasurface antennas," *IEEE Trans. Wireless. Commun.*, vol. 22, no. 1, pp. 393–407, 2023.
- [13] W. Huang, H. Zhang, N. Shlezinger, and Y. C. Eldar, "Joint microstrip selection and beamforming design for mmwave systems with dynamic metasurface antennas," in *ICASSP 2023 - 2023 IEEE International Conference on Acoustics, Speech and Signal Processing (ICASSP)*, 2023, pp. 1–5.
- [14] M. R. Castellanos, J. Carlson, and R. W. Heath, "Energy-efficient tri-hybrid precoding with dynamic metasurface antennas," in *2023 57th Asilomar Conference on Signals, Systems, and Computers*, 2023, pp. 1625–1630.
- [15] S. Yang, C. Zhang, H. K. Pan, A. E. Fathy, and V. K. Nair, "Frequency-reconfigurable antennas for multiradio wireless platforms," *IEEE Microw. Mag.*, vol. 10, no. 1, pp. 66–83, 2009.
- [16] A. Sakkas, V. Oikonomou, G. Mystridis, V. Christofilakis, G. Tatsis, G. Baldoumas, V. Tritiakakis, and S. K. Chronopoulos, "A frequency-selective reconfigurable antenna for wireless applications in the S and C bands," *Sensors*, vol. 23, no. 21, p. 8912, 2023.
- [17] H. Wang, N. Shlezinger, Y. C. Eldar, S. Jin, M. F. Imani, I. Yoo, and D. R. Smith, "Dynamic metasurface antennas for MIMO-OFDM receivers with bit-limited ADCs," *IEEE Trans. commun.*, vol. 69, no. 4, pp. 2643–2659, Apr. 2020.
- [18] 3GPP, "NR; physical channels and modulation," *3rd Generation Partnership Project (3GPP), Technical Specification (TS) 38.211*, vol. 9, 2018.
- [19] S.-H. Lee and Y.-H. Lee, "Adaptive frequency hopping for bluetooth robust to WLAN interference," *IEEE Commun. Lett.*, vol. 13, no. 9, pp. 628–630, 2009.
- [20] H. Yan, V. Boljanovic, and D. Cabric, "Wideband millimeter-wave beam training with true-time-delay array architecture," in *Proc. 53rd Asilomar Conf. Signals, Syst., Comput.*, 2019, pp. 1447–1452.
- [21] V. Boljanovic, H. Yan, C.-C. Lin, S. Mohapatra, D. Heo, S. Gupta, and D. Cabric, "Fast beam training with true-time-delay arrays in wideband millimeter-wave systems," *IEEE Trans. Circuits Syst. I: Regul. Pap.*, vol. 68, no. 4, pp. 1727–1739, 2021.
- [22] Y. Ghasempour, C.-Y. Yeh, R. Shrestha, D. Mittleman, and E. Knightly, "Single shot single antenna path discovery in thz networks," in *Proceedings of the 26th Annual International Conference on Mobile Computing and Networking*, 2020, pp. 1–13.
- [23] W. B. Davenport, W. L. Root *et al.*, *An introduction to the theory of random signals and noise*. McGraw-Hill New York, 1958, vol. 159.
- [24] J. A. Russer and P. Russer, "Modeling of noisy EM field propagation using correlation information," *IEEE Trans. Microw. Theory Tech.*, vol. 63, no. 1, pp. 76–89, 2014.
- [25] P. T. Bowen, M. Boyarsky, L. M. Pulido-Mancera, D. R. Smith, O. Yurduseven, and M. Sazegar, "Optimizing polarizability distributions for metasurface apertures with lorentzian-constrained radiators," *arXiv preprint arXiv:2205.02747*, 2022.
- [26] N. Deshpande, M. R. Castellanos, S. R. Khosravirad, J. Du, H. Viswanathan, and R. W. Heath, "A wideband generalization of the near-field region for extremely large phased-arrays," *IEEE Wireless Commun. Lett.*, vol. 12, no. 3, pp. 515–519, 2023.
- [27] M. Lin, X. Huang, B. Deng, J. Zhang, D. Guan, D. Yu, and Y. Qin, "A high-efficiency reconfigurable element for dynamic metasurface antenna," *IEEE Access*, vol. 8, pp. 87 446–87 455, May 2020.
- [28] J. Wang, W. Tang, J. C. Liang, L. Zhang, J. Y. Dai, X. Li, S. Jin, Q. Cheng, and T. J. Cui, "Reconfigurable intelligent surface: Power consumption modeling and practical measurement validation," *IEEE Trans. Commun.*, Mar. 2024.
- [29] G. C. Trichopoulos, P. Theofanopoulos, B. Kashyap, A. Shekhawat, A. Modi, T. Osman, S. Kumar, A. Sengar, A. Chang, and A. Alkhateeb, "Design and evaluation of reconfigurable intelligent surfaces in real-world environment," *IEEE Open J. Commun. Soc.*, vol. 3, pp. 462–474, Mar. 2022.
- [30] V. Va, J. Choi, T. Shimizu, G. Bansal, and R. W. Heath, "Inverse multipath fingerprinting for Millimeter wave V2I beam alignment," *IEEE Trans. Veh. Technol.*, vol. 67, no. 5, pp. 4042–4058, 2018.
- [31] P. Ramirez-Espinosa, R. J. Williams, J. Yuan, and E. De Carvalho, "Performance evaluation of dynamic metasurface antennas: Impact of insertion losses and coupling," in *GLOBECOM 2022-2022 IEEE Global Communications Conference*. IEEE, 2022, pp. 2493–2498.
- [32] N. V. Deshpande, M. R. Castellanos, S. R. Khosravirad, J. Du, H. Viswanathan, and R. W. Heath, "Achievable rate of a SISO system under wideband matching network constraints," in *GLOBECOM 2023 - 2023 IEEE Global Communications Conference*, 2023, pp. 7514–7519.